ACCEPTED FOR PUBLICATION
Robotica, Volume 36, Issue 12, December 2018, pp. 1897 – 1919. DOI: https://doi.org/10.1017/S0263574718000796

https://www.cambridge.org/core/journals/robotica/article/abs/unconventional-calibration-strategies-for-micromanipulation-workcells/E8BCE9633E4E1F9601EFAC2ADD97D8C4

Unconventional calibration strategies for micromanipulation work-cells

G. Fontana†#, S. Ruggeri†, G. Legnani‡ and I. Fassi†

† Institute of Industrial Technologies and Automation, National Research Council, Italy
‡ Department of Mechanical Engineering, University of Brescia, Italy

SUMMARY

Thise paper presents and compares a set of calibration strategies useful to calibrate vision-based robotised work-cells for micromanipulation and microassembly.

To grasp and release microparts precisely, ~~a~~ robot calibration, ~~a~~ camera calibration and ~~a~~ robot-camera registration are needed. Conventional calibration methods are very onerous at the microscale, therefore two alternative unconventional procedures, called virtual grid calibration and hybrid calibration, ~~were~~ are developed~~,~~ for work-cells with high-performance robots, minimizing ~~the~~ necessary instrumentation.

Moreover, an effective calibration of the robot end-effector ~~was~~ is designed to compensate for misalignment and orientation errors with respect to the vertical rotational axis.

~~The~~ This paper describes the calibration methods and their implementation, the results and the ~~achieved~~ improvements achieved. A detailed comparison between the hybrid and the virtual grid calibrations is provided, demonstrating the higher performance of the latter strategy.

KEYWORDS: micromanipulation; calibration; camera calibration; work-cell accuracy; 2D vision systems

1. Introduction

~~Recently,~~ Aautomated work-cells have been recently designed and used to manipulate miniaturized components for different applications in growing fields such as manufacturing and remanufacturing of electronic products, assembly of hybrid MEMS, microactuators, biomedical devices and ICT equipment [1]. These tasks require ~~a~~ precise manipulation to grasp, orient and release ~~the~~ parts~~.~~~~,~~ This manipulation ~~that~~ is in most cases ~~is~~ performed on the *x*-*y* plane.

Although ~~A~~all ~~the~~ devices composing a robotised work-cell present inaccuracies and introduce errors, ~~however~~ they have to cooperate properly. This is especially relevant when manipulating and assembling

components with sub-millimetric dimensions, in order to constitute small products. Therefore, the whole work-cell has to be calibrated. The Sstand-alone devices have to be calibrated and their relative location has to be univocally determined [2].

This paper considers the errors related to the vision systems (camera and lenses parameters and their location with respect to the robot) and to the gripper, while whereas the manipulator errors are not considered. However, the manipulator errors influence the implementation and the later exploitation of the proposed calibration methods;, therefore the robot in the work-cell has to be characterized by have good repeatability and by an accuracy which is close to the application desired final precision of the application. The Rrepeatability depends on the robot mechanical quality of the robot; it is therefore that is a design and production property and cannot be improved. If the adopted robot has is characterized by insufficient accuracy, it must be calibrated in advance with suitable procedures [3, 4, 5]. A short description of the robot errors are is briefly recalled in Appendix A. Differently, the gripper errors have instead to be considered instead to comply with the end-effector later assembly of the end-effector.

Therefore, the main ideas of this work are: i) to develop and compare two different strategies for the robot-camera calibration at the microscale, which are called *hybrid* strategy (Section 5.1) and *virtual grid* strategy (Section 5.2), showing in order to show the superior potentialities of the virtual grid approach (Section 6.3);, ii) to apply it the latest approach to both fixed (Section 6) and mobile cameras (Section 7);, and iii) to develop an effective end-effector calibration to finalize the calibration of the whole work-cell (Section 8).

The proposed non-conventional calibration strategies proposed are based on the well-knownwell-known single-plane calibration model. However, the novelty lies in the procedure and related implementation that targeted the microscale, which lacks of standard and simple procedures. Moreover, the single-plane calibration compensates for the perspective and lens distortion errors resulting in a suitable approach in all the cases where a precise manipulation is required in the *x-y* plane. These strategies can be implemented for the calibration of all serial and parallel robots having from 2 to 4 degrees of freedom (2 translations at least), mounting different types of grippers such as vacuum grippers or microtweezers.

Therefore, the innovative aspect of this paper is the conception and comparison of calibration processes to co-register all individual devices in at the same frame. The developed strategies thus developed have been then applied to the calibration of a micromanipulation work-cell, equipped with several cameras, assembly

stages~~,~~ and a high precision micromanipulator mounting a vacuum microgripper.

Thi~~s~~e paper is structured as follows. After a brief discussion ~~in Section 2~~ on the main issues related to ~~the~~ robot and camera calibration in Section 2, Section 3 presents the conventional method to calibrate ~~a~~ vision-based robotised work-cells. Section 4 describes ~~the~~ a micro work-cell. ~~Then, I~~In Section 5 the ~~proposed~~ calibration procedures for fixed cameras proposed are presented~~, while~~ whereas Section 6 discusses on their implementation in our work-cell. Section 7 reports the calibration method and implementation for on-board cameras. Finally, ~~the~~ end-effector calibration is reported in Section 8.

2. Robot and Camera Calibration issues

When a robot and a vision system have to cooperate within the same working space, ~~a~~ robot calibration, ~~a~~ camera calibration and ~~a~~ robot-camera registration are needed. Figure 1 shows the main reference systems involved during a general calibration process: the subscripts *g*, *r*, *c* and *i* respectively represent the ground, the robot base, the camera and the image ~~respectively~~. ~~The~~ 3D space coordinates are indicated by *x*, *y*, *z* and expressed in millimetres~~, while~~ whereas *u* and *v* represent ~~the~~ image coordinates and are expressed in pixels.

As said above, many applications require the manipulator to grasp and release objects on a planar surface under the supervision of a camera. In all these cases ~~a~~ 2D camera calibration, considering a single plane, is needed.

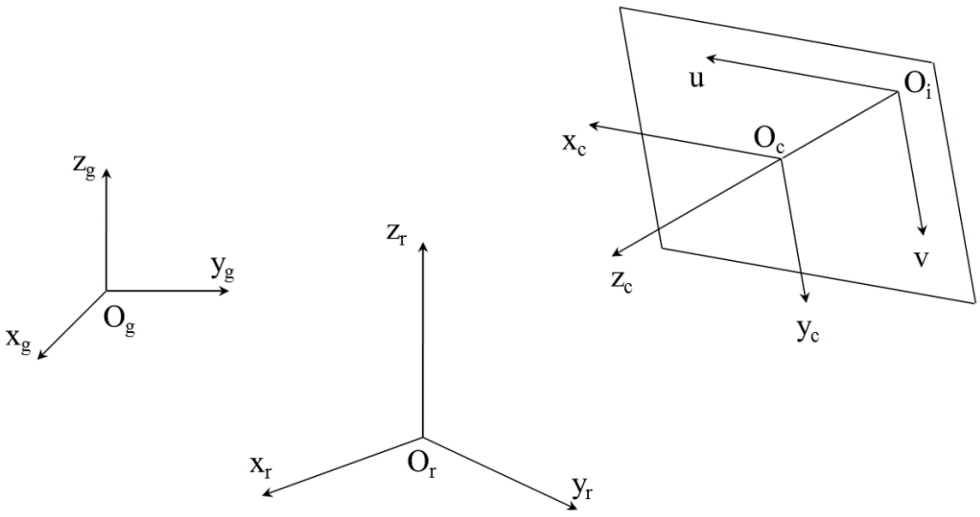

Fig. 1. Representation of the main reference frames involved in ~~the~~ calibration processes.

~~The~~ C~~c~~amera calibration has to be performed to compute image pixel to real-world unit transformation

and to compensate for perspective, distortion and spatial referencing errors [6, 7] (Fig. 2).

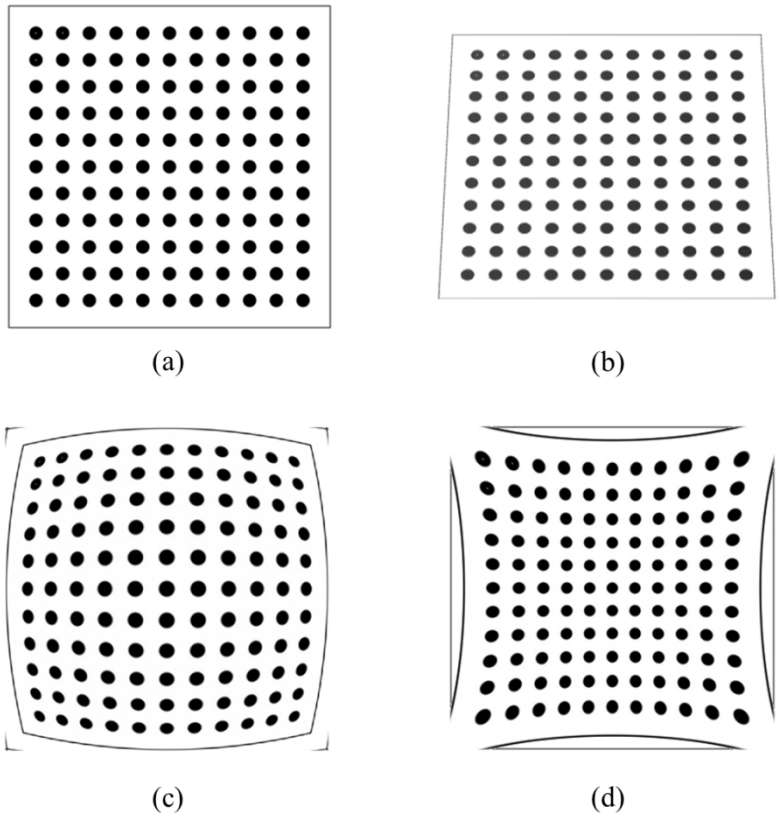

Fig. 2. Effect of different image distortions: a) actual grid; b) perspective error; c) barrel; d) pincushion. ~~The~~ A perspective error can be compensated by the model of Eq. (B1), ~~while~~ whereas radial and tangential distortion can be compensated by the model of Eq. (B2) in Appendix B.

3. The conventional calibration strategy

In order to calibrate a camera, it is necessary to compare the real coordinates (generally expressed in millimetres) of some points with their coordinates in the camera image (in pixels). This operation exploits a model of the camera and lens, by applying ~~the~~ perspective transformation, and ~~a~~ distortion compensation. It can be performed by using an object of known shape and size. Planar 2D calibration can be performed by using a grid of points (also called *markers*). Good grids containing a set of precise shapes (usually circles) at predefined known positions are generally traced on flat rigid surfaces made of material which is not sensitive to external conditions such as humidity, temperature, or other. Common surfaces are special glass or ceramic plates.

~~The~~ Ggrid quality improves with the number and ~~the~~ precision of the marked points and must fill most of the camera Field of View (FoV) ~~of the camera~~; moreover, it should be placed in focus.

The camera *x-y* reference system ~~of the camera~~ is generally established by placing its origin in the centre of one marker and the direction of one axis is chosen directing it to the centre of a second marker. The estimation of the relative pose of the camera with respect to ~~that~~ the one of the robot (registration) is performed by moving a registration object mounted on the gripper (usually a pin) to some points of the grid. The absolute positions of the points in the robot reference system are then compared with the positions of the pin with respect to the grid in the camera reference system. Finally, the corresponding transformation is estimated; 3D cases require a third point to define the direction of a second axis. The last axis direction is achieved by imposing mutual orthogonality of the axes. As explained, ~~a~~ 3D registration requires a minimum of 3 *xyz* points, ~~while~~ whereas in 2D cases 2 *xy* points are sufficient. If more points are available, ~~the~~ rototranslation can be identified with the least squares criteria. ~~The~~ C~~c~~amera and lens distortion models are reported in Appendix B.

At ~~the~~ microscale, the mentioned procedure often used in the macro domain~~,~~ is too onerous due to the characteristics of the vision system for the microscale and ~~the~~ to more demanding precision. Indeed, to achieve a high level of resolution, in order to distinguish the maximum level of detail from images, the optics of the vision system must provide ~~a~~ high magnification. This requirement causes the system to be characterized by a small field of view ~~of the system~~, thus ~~that~~ limiting~~s~~ the viewable microassembly area. Moreover, ~~the~~ high magnification requires a small working distance, which results in a small working volume for ~~the~~ manipulation. Furthermore, under normal conditions of use (air, visible light, large numerical aperture, high magnification), the depth of field is fairly small, thus limiting the applicability of stereoscopic vision techniques (3D vision) [8]. In addition, the calibration grid should be very precise (micrometric range), thus increasing its manufacturing cost. Furthermore, the registration pin must have ~~a~~ highly precise construction and its location on the gripper must be established with high accuracy.

To overcome the abovementioned problems two alternative unconventional calibration approaches (i.e. not conventional with respect to the calibration procedure used ~~in the~~at macroscale) are proposed in this paper: ~~the~~ virtual grid calibration and ~~the~~ hybrid calibration. The conceived methods ~~were~~ are implemented for the work-cell described in Section 4, but ~~they~~ are adaptable to all the robotic work-cells designed for ~~the~~ vision-based automatic manipulation on the *x-y* plane, irrespective of the kinematic structure of the manipulator, the gripper type and the overall setup.

It is important to stress that in many manipulation work-cells like the one analysed in this paper, ~~the~~ a

robot must operate with precision just in limited portions of its working space where it is necessary to register the *x-y* coordinate of the vision systems with ~~those~~ the one of the manipulator. In our case each vision system ~~had~~ has a field of view of few square centimetres (see Table I), ~~while~~ whereas the robot working area is contained in a rectangle of roughly 15 x 10 cm. When a limited working area ~~of the robot~~ is considered for the robot and ~~the robot~~ this is a precision manipulator, ~~the~~ error distribution is similar to ~~that~~ the one that can be produced by ~~a~~ rototraslation, ~~by a~~ perspective transformation or ~~by an~~ optical distortion. These errors are easily compensated by camera calibration. Moreover, ~~the~~ vision systems are generally used just to identify the pose of objects to be manipulated and not to perform any high precision dimensional analysis of ~~the~~ objects. For these reasons, ~~the~~ work-cell calibration ~~of the work-cell~~ can be performed without an external absolute reference system (e.g. a precision optical grid), but by using the robot itself as a reference. This is the principle adopted to design the virtual grid approach described in Section 5.2. After calibration, the final *x-y* coordinates of the robot and ~~of~~ the vision systems will match (even if they could be possibly ~~be~~ slightly different from ~~that~~ the ones of an external absolute reference system, ~~however not~~ without obstructing the possibility of manipulating objects). This means that the implementation of the proposed virtual grid method is able to compensate for small errors correlated with ~~the~~ robot accuracy (for significant errors ~~the~~ robot calibration is needed). However, an exception occurs when the vision system is moved within a large area of the robot working space (i.e. on-board cameras mounted on ~~the~~ a robot end-effector); in this case, the virtual grid method cannot compensate for the errors correlated with ~~the~~ robot accuracy (even if they are small).

The ~~proposed~~ hybrid calibration procedure proposed is described as a comparison in Section 5.1. The errors obtained in this case are worse, probably also because ~~the~~ robot errors cannot be compensated.

4. The work-cell for microassembly

The set-up used for ~~the~~ calibration experiments is reported in Fig.3. The hardware and software concept of the work-cell is described in more detail in [9, 10]. It consists of a high precision 4 dof robot Mitsubishi Electric [11] RP-1AH (1), with Schönflies motion [12]~~,~~ and vision systems meeting the microscale requirements of resolution, field of view, working distance, depth of field (see Table I) and gripping tools. In this case, a standard vacuum microgripper (2) with internal diameter size of 260μm ~~was~~ is used.

The robot *x-y* repeatability is ~~-~~±5 μm; its *z* repeatability is ±10 μm. The vacuum generation system (3)

exploits a vacuum ejector based on Venturi effect (3).

For the current purposes of thise work~~,~~ ~~the~~ a work-cell ~~was~~ is configured to exploit three suitable vision systems including two fixed cameras (4, 5) and an on-board camera (6), in order to measure the pose of the parts in the focal plane. The technical data of these vision systems are reported in Table I. The parts to be manipulated ~~lied~~ lie on a transparent glass substrate (7), so that the first camera detect~~sed~~ ~~from the bottom~~ their position and orientation from the bottom by means of an optical mirror. The second camera allow~~sed~~ instead a top view of the assembly area (8). The third camera ~~was~~ is mounted on the robot end-effector, thus being able to ~~and it could~~ move jointly with it and~~,~~ providing a top view of the whole working area.

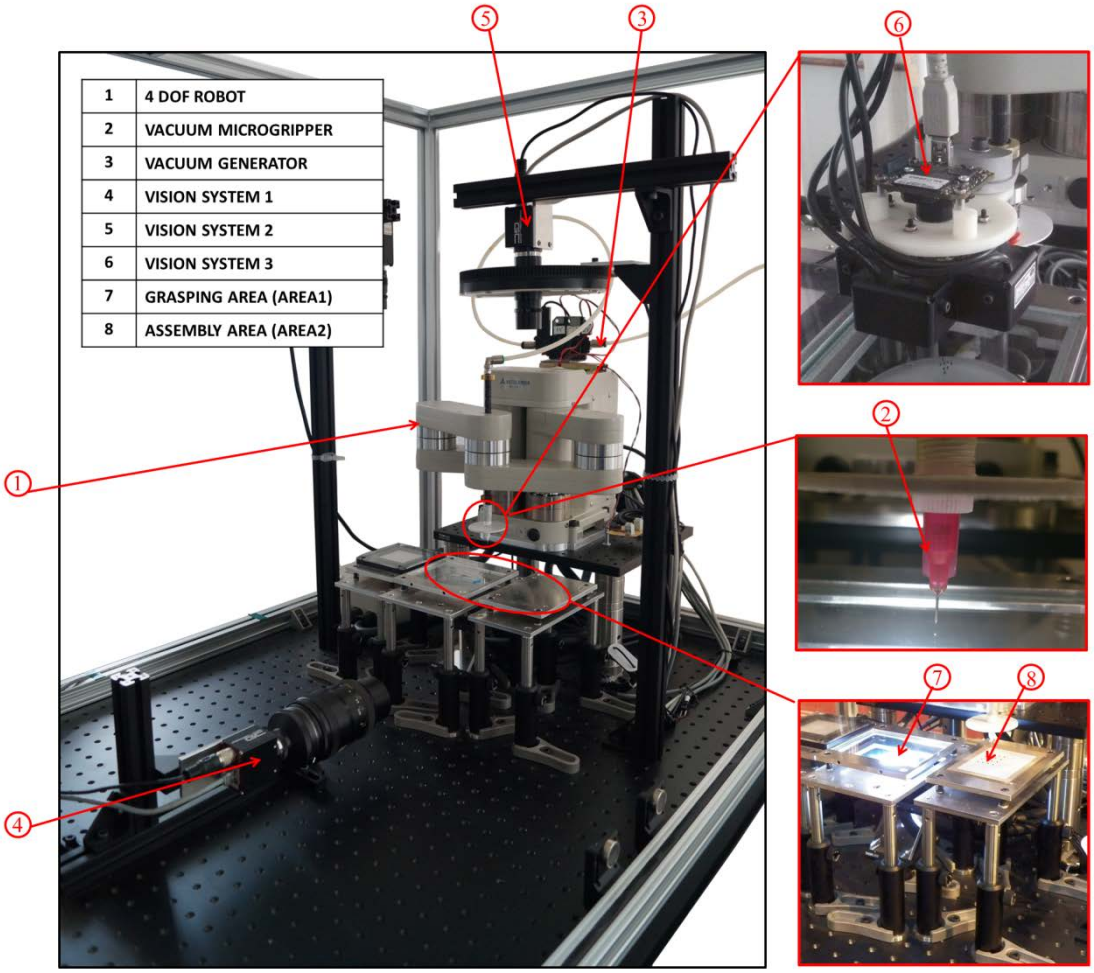

Fig. 3. The work-cell prototype ~~of the work-cell~~.

~~For the~~ As regards fixed cameras, ~~the~~ calibration consists in determining the parameters to compensate for ~~the~~ perspective transformation and ~~the~~ optical distortion. ~~For the~~As far as the mobile camera (on-board camera) is concerned, it is also necessary to determine ~~the~~ its position ~~of the camera~~ with respect to the

gripper. ~~For~~ As to the gripper, ~~the~~ misalignment and ~~the~~ orientation errors with respect to the robot vertical rotational axis ~~of the robot~~ have to be identified.

The robot operates pick-and-place operations on a number of planar surfaces which have to be orthogonal to the robot vertical motion ~~of the robot~~. Both the glass substrate and the assembly area (hereafter called area1 and area2) ~~were~~ are mounted on compliant adjustable orientation platforms, in order to set their planarity and improve ~~the~~ safety against any vertical accidental collision of the gripper on these areas. ~~The~~ Pplanarity can be verified by using a precision laser sensor mounted on the robot end-effector. Indeed, the orthogonality of the planes can be assured by adjusting the orientation of each plane by means of specific screws and it ~~was~~ is verified by scanning the plane surfaces by a laser sensor (model IL-S065 by Keyence) moved by the robot (Fig. 4); a constant distance must be obtained [13].

Table I. Technical data of the three vision systems.

	Camera Model	Lens Model (focal length f [mm])	Resolution (R) [pixel]	Field of View (FoV) [mm]	Spatial Resolution (Rs) = FoV/R [µm/pixel]
Vision System 1 (bottom view)	Allied Prosilica GC2450	Voigtländer macro lens, f=100 mm	2448x2050	16.3x13.5	6.6
Vision System 2 (top view)	Allied Prosilica GC1380H	VS Technology VS-LD75, f=75 mm	1360x1024	32.70x24.59	24
Vision System 3 (on-board camera)	Matrix Vision mvBlueFOX-MLC205C	Matrix Vision MV-O-SMOUNT-12.0IRC B5M12028C, f=12mm	2592x1944	16.23x12.14	6.2

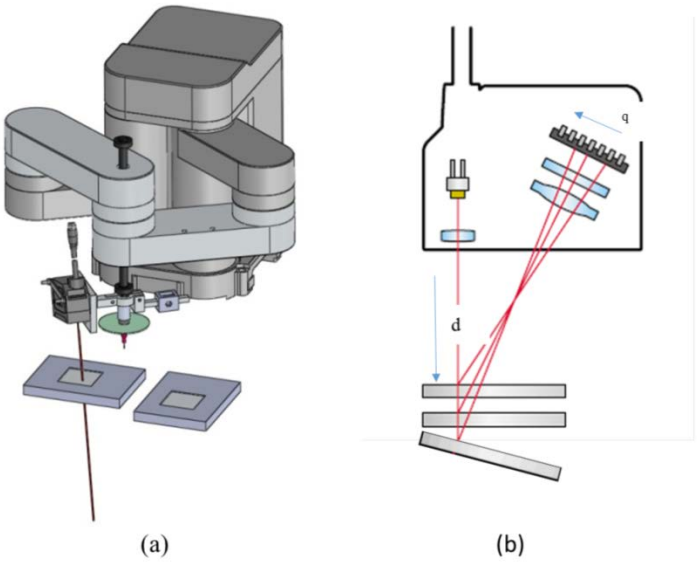

Fig. 4. ~~The~~ Use of the laser sensor to verify ~~the~~ planarity of the working areas and their orthogonality with respect to the robot vertical axis ~~of the robot~~: a) 3D model of the setup; b) the working principle based on a linear array camera which measures the position of the incident beam reflected by the target $q=f(d)$.

5. ~~The~~ Nnon-conventional calibration strategies for ~~the~~ fixed cameras

~~The~~ A manipulator has to grasp and release objects in area1 and area2 under the supervision of ~~the~~ vision systems (Fig. 3). In thise specific case, the two areas are supervised by ~~the~~ two fixed cameras, one for each zone, ~~while~~ whereas ~~the~~ an on-board camera will be considered later in Section 7. Thus, as said above, the robot has to be calibrated, as well as both the cameras~~;~~, ~~then a~~ robot-camera registration is also needed. The aim of ~~the~~ robot calibration is the improvement of its accuracy [14] and ~~was~~ is performed by measuring its actual motion [3, 15] to estimate its geometrical parameters [4, 5]. In this work, it is assumed that the robot ~~showed~~ has shown ~~a~~ suitable accuracy; therefore, this step is not discussed. However, ~~the~~ calibration of the vision systems ~~was~~ is necessary and ~~a~~ 2D calibration ~~was~~ is considered appropriate. Two different calibration strategies are proposed (main idea i in Section 1): the former represents an adjustment of the standard method, thus called hybrid strategy, ~~while~~ whereas the latter is a fully non-traditional method and is~~,~~ named virtual grid strategy. It is worth ~~to note~~noting that they are two alternative strategies to calibrate vision-based robotised work-cells for micromanipulation and microassembly~~;~~, therefore they are not combinable.

5.1 Hybrid calibration strategy

~~The~~ ~~C~~camera calibration is performed by means of an actual grid of dots printed on a substrate and placed on ~~the~~ a camera focal plane. The ~~developed~~ vision algorithms developed calculate in pixels the set of ~~barycenters~~barycentres of the dots ~~in pixels~~ that, together with the corresponding set in millimetres, is processed by the camera calibration algorithm.

~~Then~~Afterwards~~,~~ ~~the~~ registration between the robot base frame and the camera frame is needed.

Performing ~~a~~ registration in the standard way is very challenging at ~~the~~ microscale, due to ~~the~~ a high-demanding positioning of the pin mounted on the end-effector on the grid points ~~of the grid~~. Thus, depending on the configuration of the camera to be calibrated, two alternative approaches have been adopted.

Concerning area1, ~~the~~ referencing is obtained by moving the gripper in the field of view of the camera in n known positions ($n \geq 2$). When ~~the~~ a gripper nozzle cannot be easily recognized by the camera, a sphere gripped by the robot end-effector can be used. Similarly, in area2 ~~the~~ registration of the second camera frame with respect to the robot frame is obtained by commanding the robot to place n spheres in the camera FoV ~~of the camera~~ in known positions. In both cases, the positions of the spheres are measured by the related camera by using its reference system and the corresponding transformation between the two systems is computed. Moreover, the rotation of the vertical axis has to be kept constant to avoid the influence of misalignment and orientation errors with respect to the vertical rotational axis of the robot (see Section 8).

5.2 Virtual grid calibration strategy

The virtual-grid calibration strategy is a methodology to simultaneously perform ~~the~~ calibration of the camera and its registration with respect to the robot reference system without using any additional tools or sensors. The procedure is theoretically justified by the assumption that the robot positioning error is negligible, but in practice thi~~s~~e procedure also compensates ~~also~~ for small robot errors.

The physical grid is replaced by a "virtual grid" realized by objects placed by the robot in N=RxC known xy absolute positions (where R and C are the number of the rows and columns of the grid of points). In some cases, the gripper itself can suffice.

In practice, to calibrate the first camera (bottom view), the gripper is sequentially moved to the set of N positions where a picture is taken and the position of the gripper (or of the object that the gripper holds) is

measured by the vision system. In more detail, the procedure develops as follows. At the ~~start~~beginning~~,~~ the gripper is moved to the first x-y position (P_1), the camera takes a bottom picture of the gripper~~,~~ and the gripper position is measured. The pair of image coordinates and the gripper absolute coordinates ~~of the gripper~~ are stored. The gripper is then moved in the *x*-*y* plane of a specified offset to reach position P_2. The camera takes a second picture and the gripper position is derived. These steps are repeated until the set of N grid positions is complete (see Fig. 5 and Fig. 6). The set of collected data is then elaborated by using the same principle of an ordinary grid, Eq.s (B1) and (B2) in Appendix B, thus compensating for distortion and perspective errors. A similar procedure is described in [16]. To facilitate the measur~~e,~~ing, the grasped object must have a simple shape~~,~~ and ~~it~~ must be able to auto-centre on the gripper, to increase ~~the~~ accuracy; for these reasons, a sphere can be considered suitable. When the gripper has a simple shape (e.g. a round nozzle), the bare gripper can be used for thi~~s~~e calibration procedure. It is worth ~~to note~~noting that the order of the collected data does not affect ~~the~~ calibration precision, since the multidirectional positioning error is ~~less than~~inferior to ~~the~~ robot repeatability (5 μm in the *x*-*y* plane).

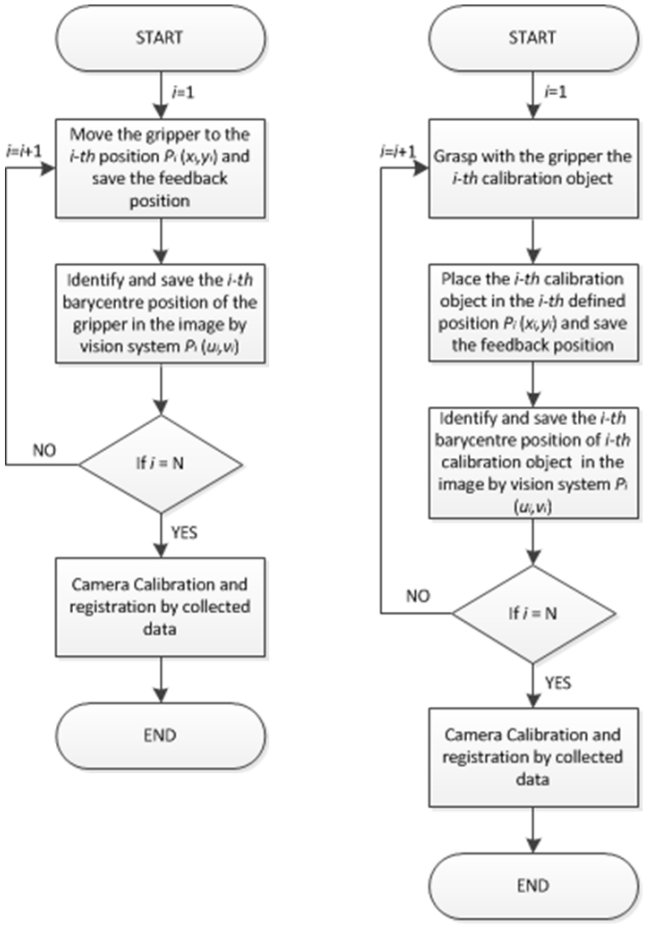

(a) (b)

Fig. 5. Flowcharts illustrating the steps of virtual grid calibration ~~the~~ implementation ~~of the virtual grid calibration~~: a) for area1; b) for area2.

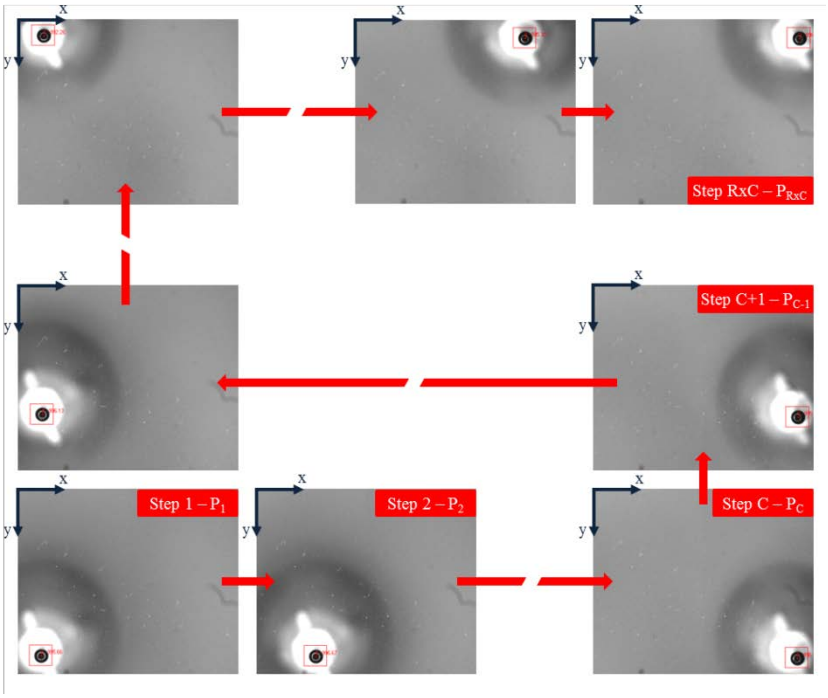

Fig. 6. Schematic representation of the different steps of ~~the~~ virtual grid calibration in area1.

~~For~~ As regards the second camera (top view), the procedure must be adapted because of the presence of the robot itself in the camera field of view ~~of the camera~~. In this case~~,~~ the robot is employed to grasp several objects and place them in the camera FoV ~~of the camera~~, in predefined N=RxC positions, to form a grid (see Fig. 7). In our case~~,~~ small spheres ~~has been~~are placed on an adhesive surface to avoid undesired part rolling. Figure 5 shows the flowcharts of the described virtual grid calibration strategies for area1 and area2.

In both cases~~,~~ the gripper ~~was~~ is kept with constant orientation (no rotation around the vertical axis) to avoid any effects due to the geometrical inaccuracy of the gripper itself, that will be considered in Section 8.

This procedure does not require ~~the~~ any use of expensive calibrated grid, or any other calibration tools, and ~~the~~ final precision depends only on the vision system spatial resolution ~~of the vision system~~ and the encoder resolution of the robot.

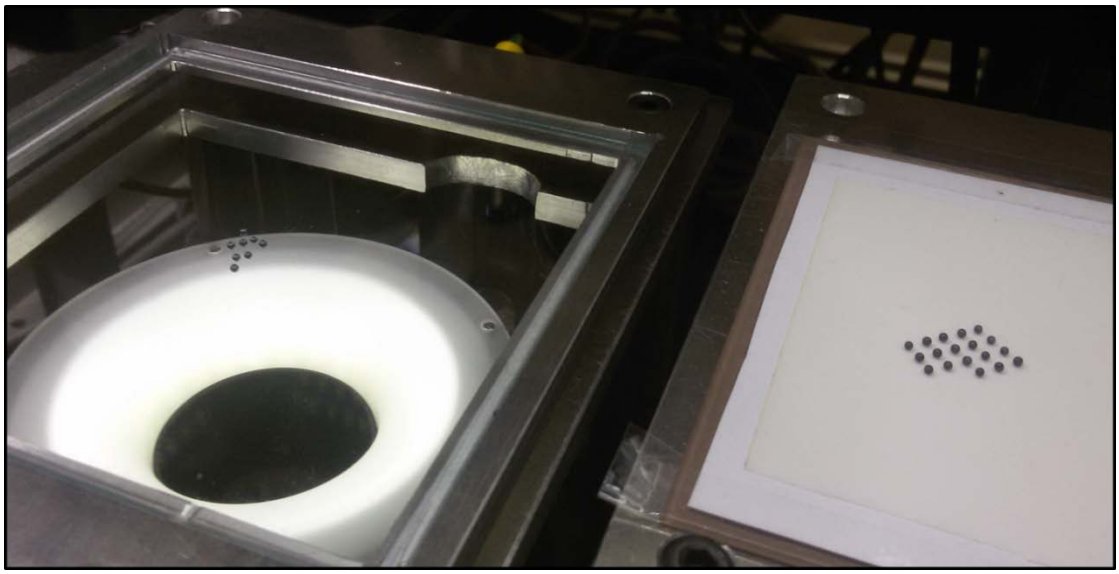

Fig. 7. Calibration of the second camera. On the left, ~~the~~ area1 used as a gripping area seen by the first camera; on the right, ~~the~~ virtual grid ~~is in~~under construction in area2.

5.3 Performance evaluation

The verification test to measure the effectiveness of the different calibration procedures ~~was~~ is performed by asking the robot to place some objects (e.g. the gripper nozzle or some spheres) in known *xy* positions within the camera FoV ~~of camera~~, by measuring their positions by means of a comparison if~~comparing~~ the known positions with the measured ones. The objects ~~were~~ are placed in verification positions different from ~~those~~ the ones used for ~~the~~ calibration.

For the sake of completeness, this calculation has been computed also for the points used for ~~the~~ registration in the hybrid process and for the virtual grid construction in the second process. The chosen performance index ~~was~~ is the radial position error e, defined as:

$$e = \sqrt{(x_a - x_d)^2 + (y_a - y_d)^2}$$

where x_a , y_a are the actual coordinates of the gripper nozzle or sphere centre ~~of the gripper nozzle or sphere~~ and x_d , y_d are the coordinates measured by the calibrated camera. Fig. 8 shows the radial position error (e) in the calibration points of area2 represented by arrows: errors have been amplified for a clear visualisation.

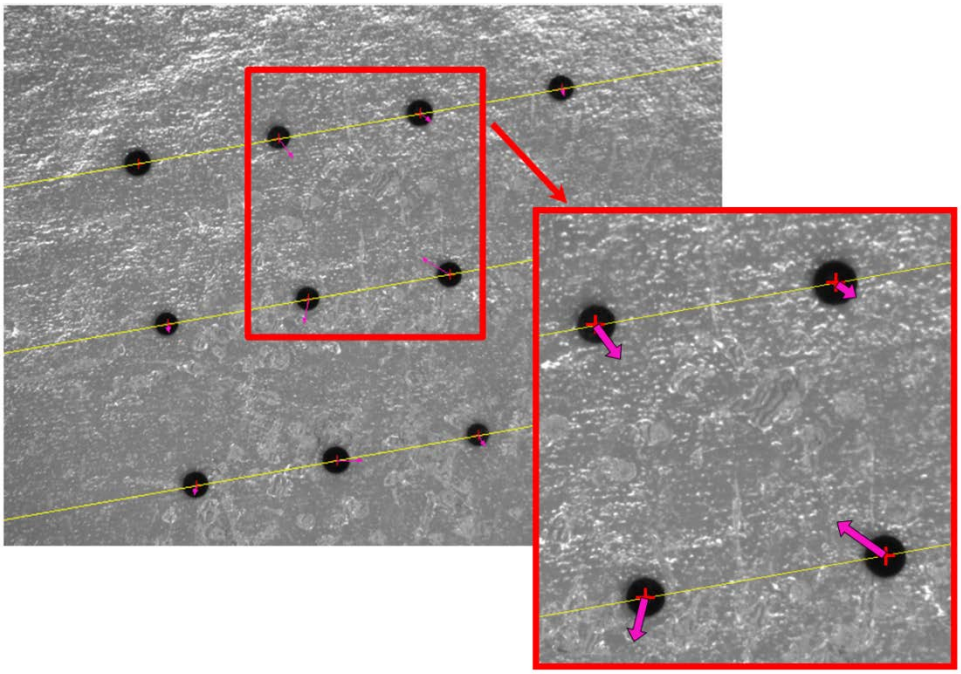

Fig. 8. Representation of the radial position error *e* in the calibration points of area2.

6. Implemented calibration strategies

6.1 Calibration of area1

In this Section~~,~~ the implementation of the two different approaches to the calibration of the first camera and its registration with respect to the robot base frame are presented.

6.1.1 Hybrid strategy

As prefaced in Section 3, ~~the~~ camera calibration is performed by means of an actual grid. In this case, a grid of 8x7 black dots printed on a white substrate with a diameter of 1 mm, a dot spacing of 2 mm and a dot spacing tolerance of 5 µm ~~was~~ is adopted. The grid ~~was~~ is fixed on the glass substrate and placed to be seen in focus. The camera ~~took~~ takes a picture of the grid and the vision algorithm provide~~d~~s for the identification of the dots and the calculation of their barycentres.

The origin of the calibration grid coordinate system ~~of the calibration grid was~~ is set to coincide with the barycentre of the top left dot~~,~~; the *x*-axis ~~was~~ is aligned with the topmost row of dots and the *y*-axis ~~was~~is orthogonal and directed downwards in the image. In this way~~,~~ the two sets of barycentre positions expressed in millimetres and pixels ~~could~~ can be processed by ~~the~~ a calibration algorithm. ~~Then~~Afterwards, the

algorithm performsed the transformation and compensatesd for perspective and distortion errors. For this work, all the vision algorithms were are developed using LabView™; its vision libraries are based on the concept of Eq.s (B1), (B2) [17] and provide a calibration function where different types of error compensation can be selected. In this case, aiming at the highest vision system performance, a kind of calibration taking into account both perspective and distortion errors was is chosen).

To perform the registration, the robot graspsed a glass sphere of about 1 mm diameter (with a diameter tolerance of ±0.2 mm) and movesd it to $n = 4$ ($n \geq 2$) known positions in the x-y plane. For all these positions, the z height was is kept constant and suchso that the sphere could can be seen in focus: in this way, the offset between the registration and calibration planes fell falls into the camera depth of field, which had has the an order of magnitude of 1 mm for the first camera. At each position, the robot stopsped, the feedback position was is sent from the robot controller to the master personal computer and the camera took takes an image. The developed vision algorithm provideseed for the identification of the sphere in the FoV. Then, the algorithm performsed the calculation of its barycentre in pixels and, since the camera was is already calibrated, even also in millimetres. Therefore, the corresponding transformation between the camera and the robot reference systems could can be computed by estimating the parameters (ϑ, x_0, y_0) of the planar rototranslation matrix between the two reference systems, represented by the following relation:

$$\begin{bmatrix} x_r \\ y_r \end{bmatrix} = \begin{bmatrix} \cos(\vartheta) & -\sin(\vartheta) \\ \sin(\vartheta) & \cos(\vartheta) \end{bmatrix} \begin{bmatrix} x_c \\ y_c \end{bmatrix} + \begin{bmatrix} x_0 \\ y_0 \end{bmatrix} \qquad (1)$$

At first, an initial estimation ϑ_e of the angle ϑ is obtained by considering the coordinates of two points of the grid measured in the camera and in the robot space:

$$\vartheta_e = atan2(y_{r2} - y_{r1}, x_{r2} - x_{r1}) - atan2(y_{c2} - y_{c1}, x_{c2} - x_{c1})$$

where atan2(y, x) is the 4-quadrant extension of arctan(y/x). Then, a first estimation of x_0, y_0 is obtained by the coordinate of one point in the grid and the robot space as:

$$\begin{bmatrix} x_0 \\ y_0 \end{bmatrix} = \begin{bmatrix} x_r \\ y_r \end{bmatrix} - \begin{bmatrix} \cos(\vartheta_e) & -\sin(\vartheta_e) \\ \sin(\vartheta_e) & \cos(\vartheta_e) \end{bmatrix} \begin{bmatrix} x_c \\ y_c \end{bmatrix}$$

The estimation is then improved by an iterative procedure which considers all the points of the grid. Linearizing Eq. (1) in the neighbourhood of $\vartheta = \vartheta_e$ (where ϑ_e is the first estimation of the angle ϑ), one obtains:

$$\begin{bmatrix} x_r \\ y_r \end{bmatrix} = \begin{bmatrix} (-\sin(\vartheta_e)x_c - \cos(\vartheta_e)y_c) & 1 & 0 \\ (\cos(\vartheta_e)x_c - \sin(\vartheta_e)y_c) & 0 & 1 \end{bmatrix} \begin{bmatrix} \Delta\vartheta \\ x_0 \\ y_0 \end{bmatrix} + \begin{bmatrix} \cos(\vartheta_e)x_c - \sin(\vartheta_e)y_c \\ \sin(\vartheta_e)x_c + \cos(\vartheta_e)y_c \end{bmatrix}$$

that for the *i-th* point of the grid can be synthetically written as:

$$B_i = \begin{bmatrix} x_{ri} \\ y_{ri} \end{bmatrix} - \begin{bmatrix} cos(\vartheta_e)x_{ci} - sin(\vartheta_e)y_{ci} \\ sin(\vartheta_e)x_{ci} + cos(\vartheta_e)y_{ci} \end{bmatrix}$$

$$A_i = \begin{bmatrix} (-sin(\vartheta_e)x_c - cos(\vartheta_e)y_c) & 1 & 0 \\ (cos(\vartheta_e)x_c - sin(\vartheta_e)y_c) & 0 & 1 \end{bmatrix}$$

$$L = \begin{bmatrix} \Delta\vartheta \\ x_0 \\ y_0 \end{bmatrix}.$$

All the *n* collected data are then grouped in the matrices *A* and *B*:

$$B = \begin{bmatrix} B_1 \\ \vdots \\ B_i \\ \vdots \\ B_n \end{bmatrix} \qquad A = \begin{bmatrix} A_1 \\ \vdots \\ A_i \\ \vdots \\ A_n \end{bmatrix}.$$

Therefore, by applying the Least Square Method to the collected data, it is possible to derive the estimated values of the vector parameters $L = [\Delta\vartheta, x_0, y_0]^T$ from equation:

$$L = (A^T A)^{-1} A^T B = A^+ B$$

where A^+ is the Moore-Penrose pseudoinverse matrix of the coefficient matrix *A* (2*n* x 3) and *B* is the (2*n* x 1) vector of the known terms. Therefore, we ~~get~~ obtain $\vartheta = \vartheta_e + \Delta\vartheta$. Since ~~the~~ linearization introduces errors, the estimation of $\Delta\vartheta$, x_0, y_0 can be reiterated to improve ~~the~~ calibration.

Moreover, to avoid the effects of ~~the~~ geometric errors at the end-effector, the rotation of the vertical axis

~~was~~ is kept constant to an angle $\alpha = \alpha_{cal}$ during this phase. ~~The~~ Ggeometric errors at the end-effector will be considered in Section 8.

The results obtained with this approach are reported in Table II, which shows the absolute values of the mean and maximum errors and the RMS error.

6.1.2 Virtual grid strategy

As described above, the procedure ~~was~~ is based on the use of a virtual grid. The robot ~~was~~ is firstly commanded to position the gripper nozzle or the sphere to be seen in focus by the camera. After that, the cycle of movements and images captures start~~ed~~, until the grid ~~was~~ is complete. Again, a grid of 8x7 positions ~~was~~ is used and ~~the~~ end-effector orientation ~~was~~ is kept constant.

As for ~~the~~ hybrid strategy, the positions of the barycentres of the gripper nozzle or the sphere ~~were~~ are identified and, again, the origin of the coordinate system of the calibration grid ~~was~~ is set to coincide with the barycentre of the top left dot. However, in this case, ~~such~~ this point corresponds to a specific position achieved by the robot, thus ~~the~~ registration between the robot and camera reference frames is simultaneously provided.

The statistical information of mean, maximum and RMS errors calculated for a single complete grid is reported in Table II. Both the results for the points used for ~~the~~ calibration and ~~of~~ verification points are reported.

6.2 Calibration of area2

Hereby, the hybrid and “virtual grid” strategies are addressed for ~~the~~ calibration and referencing of the camera providing a top view of the assembly area.

6.2.1 Hybrid strategy

The same physical standard grid used for the first camera ~~was~~ is adopted. The camera ~~took~~ takes a picture of the 16x12 black dots grid which ~~was~~ is processed by the vision algorithm.

The registration of the camera frame with respect to the robot frame ~~was~~ is then obtained by commanding the robot to place $m = 4$ ($m \geq 2$) spheres in the camera FoV ~~of the camera~~ in unaligned positions.

To accomplish this task, the first already calibrated camera ~~was~~ is exploited to provide ~~to~~ the robot with the *x*-*y* coordinates in its reference system of the spheres lying in area1.

The robot then pick~~sed by vacuum~~ and place~~sd~~ the spheres in the specified positions of the second camera FoV ~~of the second camera~~. The spheres barycentres ~~were~~ are then calculated in the camera reference frame and ~~the~~ transformation with respect to the robot frame ~~could~~ can be computed.

The procedure for the evaluation of the calibration error for the second camera ~~was~~ is identical to the previous one. ~~The~~ C~~c~~alibration quality ~~was~~ is checked by placing some spheres in some points different from ~~those~~ the ones used for ~~the~~ registration and the measuring error ~~was~~ is evaluated. Table II reports the ~~obtained~~ results obtained.

6.2.2 Virtual grid strategy

In practice, the process to create the grid of spheres ~~was~~ is similar to the approach used for the first camera registration. A grid of 4x3 dots ~~was~~ is considered as suitable, since it provide~~sd more than a sufficient~~ an amount of data which is more than a sufficient and a~~n~~ relatively low execution time ~~relatively low~~, which is an important aspect if ~~a~~ re-calibration of the system is frequently needed ~~frequently~~. The robot pick~~sed~~ and place~~sd~~, one by one, the spheres in the FoV of the camera to be calibrated. For each sphere deposition~~,~~ the camera ~~took~~ takes a picture of the under-construction grid. Once the~~This~~ last placed sphere ~~was~~ has been detected~~, and~~ its pixel barycentre ~~was~~ is calculated. The data ~~were~~ are then used to calibrate the second camera by applying the same mathematical approach used for the first camera. The position errors obtained with this strategy are reported in Table II.

Table II. Results of ~~the~~ calibration strategies applied to area1 and area2. * The number in parentheses represents the points used for ~~the~~ registration in ~~the~~ case of ~~the~~ hybrid calibration (*n* for area1 and *m* for area2).

		Error in calibration points [µm]				Error in non-calibration points [µm]			
		Mean error	Max error	RMS error	N. of points	Mean error	Max error	RMS error	N. of points
Area 1	Hybrid C.	15.2	43.2	10.5	56(+4*)	14.2	50.4	11.9	56
	Virtual Grid C.	3.9	8.8	1.7	56	6.3	19.0	3.1	
Area 2	Hybrid C.	67.5	128.3	36.0	192(+4*)	62.7	103.1	31.5	12
	Virtual Grid C.	6.8	20.8	4.8	12	19.5	46.2	12.3	

6.3 Comparison between hybrid and virtual grid calibration strategies

Concerning the unconventional calibration methods applied to the different areas, the ~~obtained~~ results obtained are reported in Table II. As one can notice, the virtual grid strategy is more effective than the hybrid one, ~~both~~ in terms of both mean, maximum and RMS errors. The mean error in the verification positions with the virtual grid approach applied to area1 is less than half of ~~that~~ the one obtained with the hybrid approach. The same error for area2 is even 3 times lower.

An analysis of the two calibration strategies leads to ~~the~~ an evaluation of the different sources of errors. Concerning ~~the~~ hybrid calibration, the total error is given by ~~the~~ a combination of errors deriving both from ~~the~~ camera calibration and from its registration. In particular, ~~the~~ camera calibration is affected by the dot spacing tolerance of the grid and by the error committed by the vision algorithm ~~which detects~~detecting the dot barycentres. In ~~the~~ registration~~,~~ a considerable error arises ~~since there is~~because of an offset between ~~the~~ registration and the calibration planes, which cannot be neglected without the use of high-precision devices. This ~~contributes~~ makes the mean and maximum errors in the registration points to be comparable with ~~those~~ the ones in non-registration points, oppositely to what happens in the ~~case of the~~ virtual grid strategy case. Moreover, the use of the robot to move the gripper nozzle or the spheres involves a further error due to the encoder resolution affecting the robot feedback position reading~~,~~ ~~and~~ besides robot geometric errors. Again, an error associated to the barycentre identification (of the gripper nozzle or the sphere) by the vision algorithm occurs. In the specific case of the first camera, a small error in the auto-centring of the sphere gripped by the robot end-effector can affect the process. When the gripper nozzle is easily recognized by the camera and~~, therefore~~ the sphere is not necessary, this error does not arise. In the second camera ~~the~~ case ~~of the second camera,~~ the auto-centring error adds to the error in positioning the sphere on the adhesive substrate caused by ~~the~~ a subtle collision between the gripper and the substrate itself.

On the other side, since in the virtual grid calibration strategy ~~the~~ camera calibration and its registration are performed simultaneously, ~~less~~ fewer sources of error than in the previous strategy arise. In this case, errors due to ~~the~~ encoder resolution and ~~to the~~ vision algorithm performance occur. The error associated to the sphere auto-centring ~~of the sphere~~ can ~~add~~ occur when the first camera is calibrated, and, ~~for~~ as regards the second camera, ~~the~~ an additional error in positioning the spheres arises.

To support the calibration of area2, it ~~was~~ is ~~decided~~ established that the already calibrated camera 1 be~~to~~ exploited ~~the already calibrated camera 1~~: on the other hand, a mechanically fixed reference place

where spheres are picked up ~~could~~ can also be adopted. This choice ~~was~~ is done to neglect the use of external devices.

It is worth ~~to note~~noting that the gripper nozzle diameter and the sphere diameter are not influential parameters and ~~they~~ do not need to be precisely known in advance. Only in the case of ~~the~~ area2 calibration ~~of area2~~, it is essential to check the sphere diameter in order to avoid mechanical interference among the placed spheres.

~~With~~ By applying the virtual grid method ~~applied~~ to fixed cameras, high precision can be achieved ~~even if the~~ despite ~~manipulator has~~ small errors of the manipulator (influencing ~~the~~ accuracy), since this method provides a “mapping” between the robot and the camera reference systems. On the other side, even if the hybrid method is affected ~~even~~ by small robot errors, ~~then the~~ its precision ~~of the method~~ can be improved by ~~a~~ preliminary robot calibration, if needed.

To conclude this discussion about ~~the~~ different calibration strategies, besides a performance analysis in terms of precision, ~~an~~ investigation on the feasibility of ~~the~~ calibration~~s~~ execution is fundamental. Comparing the two strategies in terms of execution time, the virtual grid approach is slower than the other one, since ~~the~~ grid construction takes time: with reference to the area1 calibration ~~of area1~~, ~~while~~ if the execution of the hybrid strategy ~~took~~ takes some seconds (8 seconds in the case of 4 registration points), the construction of a 8x7 virtual grid ~~took~~ takes about 2 minutes. This difference is due to the definitely fewer positions needed for ~~the~~ registration than for the virtual grid calibration strategy, since the necessary time ~~needed~~ for taking an image of the physical grid of dots is negligible. Furthermore, the necessary time ~~necessary~~ to calibrate area2 is always much higher than ~~that~~ the one needed to calibrate area1, regardless of the ~~adopted~~ method adopted, since both ~~the~~ virtual grid construction and ~~the~~ registration derive from a pick and place operation. For example, in the case of a 4x3 virtual grid construction in area2, ~~the~~ execution time ~~was~~ is about 3 minutes (note that, compared to the virtual grid of area1, 50% more time ~~was~~ is necessary to build a grid of one-fifth of positions). As to ~~the~~ hybrid strategy, the registration of area2 by using 4 positions ~~took~~ takes about one minute, that is eight times more than ~~that of the~~with the first one. In all cases, note that ~~the~~ time can vary depending on how fast the vision system recognizes the spheres.

The economic aspect is also relevant: an accurate actual grid can be expensive~~;~~, ~~thus~~ the hybrid approach thus requires higher costs than the virtual grid strategy. Indeed, the price of a commercial grid can be two orders of magnitude higher than ~~that~~ the one of some glass spheres.

7. On-board camera c~~C~~alibration ~~of the on-board camera~~

As described in Section 4, the work-cell is equipped with a mobile camera mounted on the robot end-effector. In order to exploit this additional vision system, ~~a~~ camera calibration and ~~a~~ robot-camera registration are required. If the camera pose ~~of the camera~~ is known with respect to the gripper, when the camera measures the relative positions of some points (in millimetres), it is possible to determine the absolute position of those points. Ideally, the camera rotates ~~about~~ around a vertical axis centred in the nominal gripper position. ~~While~~ Whereas we may assume by the construction of ~~the~~ a precision manipulator and by the working planes planarity ~~of the working planes~~ (see Section 4) ~~we may assume~~ that the axis is vertical, we cannot assure that thise axis ~~passes~~ crosses exactly ~~for~~ the gripper nominal centre ~~of the gripper~~. The *D* location ~~*D*~~ of the vertical axis is ~~then~~ thus to be determined. This is a simplified case of the more general case of solving the well-known $AX=XB$ problem [18].

For this camera, only the virtual strategy ~~was~~ is implemented since it ~~led~~ leads to better results, if compared with the hybrid one (main idea ii in Section 1). The procedure to collect the data ~~was~~ is very similar to ~~that~~ the one adopted by the second vision system for area2. Indeed, even in this case, the robot ~~was~~ is commanded to place a grid of n spheres on the robot working area.

The robot ~~was~~ is then moved to a position P_1 (x_{g1}, y_{g1}, α_1). A picture of the grid is taken and, for each point, the corresponding coordinates in the robot space (x_i, y_i) and in the camera space (u_{1i}, v_{1i}) ~~were~~ are collected.

~~Then~~ T~~t~~he robot ~~was~~ is then moved to a second position P_2 (x_{g2}, y_{g2}, α_2) with a second rotation angle ($\alpha_1 \neq \alpha_2$);~~,~~ a second picture ~~was~~ is taken and a new measure of the camera coordinates of the points (u_{2i}, v_{2i}) ~~was~~ is collected. It is worth ~~to note~~noting that $\Delta\alpha = \alpha_2 - \alpha_1$ should have a value to make the effect of the rotation clearly visible ~~the effect of the rotation,~~ e.g. $\Delta\alpha > 10°$.

The relative frames are defined in Fig. 9.

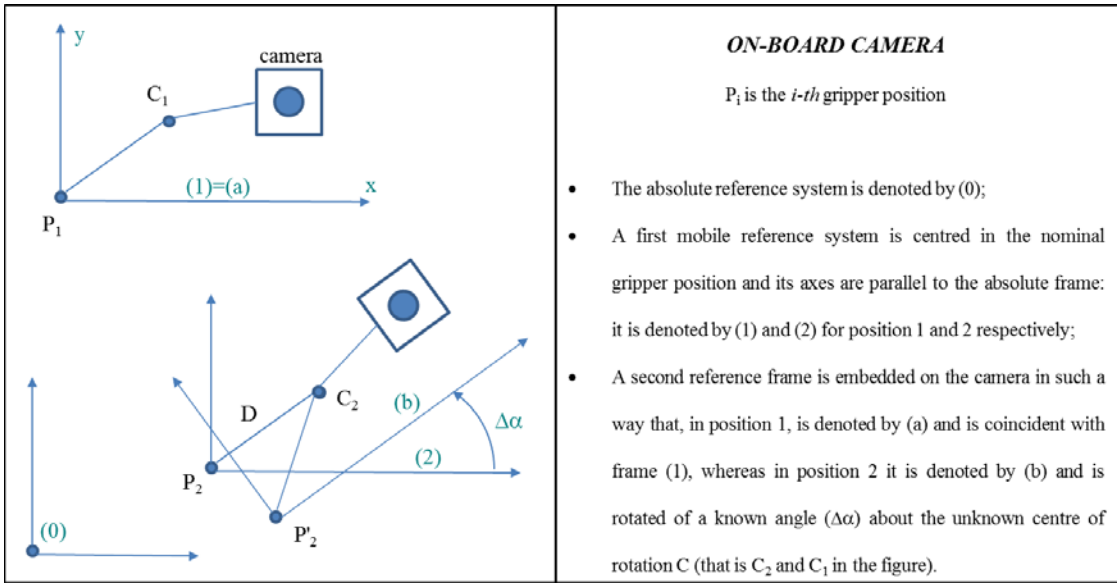

Fig.9. Definition of the reference frames for ~~the~~ on-board camera calibration.

The relative position of the *i*-th point with respect to the gripper in position 1 is:

$$A_{(1)i} = \begin{bmatrix} x_{r1i} \\ y_{r1i} \end{bmatrix} = \begin{bmatrix} x_i - x_{g1} \\ y_i - y_{g1} \end{bmatrix}$$

~~The~~ Ce~~c~~amera parameters can be obtained by the data $A_{(1)i}$ and (u_{1i},v_{1i}) collected in pose 1.

Using these parameters and the camera coordinates (u_{2i}, v_{2i}) of the points in pose 2, ~~the~~ a new relative position $A_{(2)i}$ of the points with respect to the camera ~~are~~ is obtained.

Considering the first gripper pose, the absolute position of the grid point ~~of the grid~~ is:

$$A_{(0)i} = P_1 + A_{(a)i}$$

And, considering the second gripper pose, it is also:

$$A_{(0)i} = P'_2 + RA_{(b)i} \qquad (2)$$

$$P'_2 = C_2 + R(P_2 - C_2) \qquad (3)$$

where the rotation matrix R is:

$$R = \begin{bmatrix} cos(\Delta\alpha) & -sin(\Delta\alpha) \\ sin(\Delta\alpha) & cos(\Delta\alpha) \end{bmatrix}$$

and the *D* location ~~*D*~~ of the vertical axis is:

$$D = C_1 - P_1 = C_2 - P_2 \, .$$

Therefore, by representing the 2x2 identity matrix ~~by~~ with *I* ~~the 2x2 identity matrix~~, one obtains:

$$(R - I)D = P_2 - P_1 + RA_{(b)} - A_{(a)} \qquad (4)$$

and the unknown *D* can be finally found by:

$$D = (R - I)^{-1}(P_2 - P_1 + RA_{(b)} - A_{(a)})$$

with:

$$R' = R - I = \begin{bmatrix} cos(\Delta\alpha) - 1 & -sin(\Delta\alpha) \\ sin(\Delta\alpha) & cos(\Delta\alpha) - 1 \end{bmatrix} \qquad (R - I)^{-1} = \frac{1}{2}\begin{bmatrix} -1 & -\frac{sin(\Delta\alpha)}{cos(\Delta\alpha)-1} \\ \frac{sin(\Delta\alpha)}{cos(\Delta\alpha)-1} & -1 \end{bmatrix}.$$

If more than two poses are considered, and/or more points are considered for each pose, Eq. (4) can be written for any combination of point and pose, and the equations can be grouped obtaining an over-constrained linear system to be solved with the least square criteria:

$$\bar{R}\, D = \bar{H} \qquad with \qquad \bar{R} = \begin{bmatrix} R_1 - I \\ \vdots \\ R_k - I \\ \vdots \end{bmatrix} \quad \bar{H} = \begin{bmatrix} \vdots \\ P_k - P_1 + R_k A_{(b)k} - A_{(a)k} \\ \vdots \end{bmatrix}$$

$$D = (\bar{R}^{\,T}\bar{R})^{-1}\bar{R}^{\,T}\,\bar{H} = \bar{R}^{\,+}\,\bar{H}$$

where $\bar{R}^{\,+}$ is the Moore-Penrose pseudoinverse of $\bar{R}$.

After calibration, the absolute position of any point *j* measured for any gripper pose *k* may be performed

by combining Eq. (2) and (3):

$$A_{(0)j} = P_k + (I - R_k)D + R_k A_{(b)j} \qquad (5)$$

The centre of the rotations ~~was~~ is estimated six times (Table III). In five cases (*c2*-*c6*) the estimation ~~was~~ is based on one of the poses *p2*-*p6* with respect to the first pose *p1*, used for ~~the~~ camera calibration and registration, so that ~~the~~ case c_l refers to the pose p_l , with l=2, ..., 6. In the last case (*c**) all the poses ~~were~~ are considered and the centre ~~was~~ is estimated with the least square criteria considering all the five poses (*p2*-*p6*).

Table III. E~~The e~~stimated centres of ~~the~~ rotation.

D	*c**	*c2*	*c3*	*c4*	*c5*	*c6*
x [µm]	-0.6	90.1	25.9	-26.2	53.2	-12.4
y [µm]	213.7	286.7	207.7	198.3	222.8	248.2

Tables IV, V and VI report the results of a calibration test based on 6 poses and 20 points for each pose (Fig. 10). The performance ~~were~~ is tested by applying an error index based on Eq. (5):

$$E_{jk} = P_k + (I - R_k)D + R_k A_{(b)j} - A_{(0)j}$$

As shown in the tables, the centre of the rotation determined by considering just one pose (cases *c2*-*c6*) allows for better results on that individual pose (see the combination c_l , p_l on the diagonal highlighted in the tables). However, the rotation centre ~~of rotation~~ determined with the least square criteria on all the poses (case *c**), on average, performs better. Its error is ~~near~~ close to the minimum and generally far from the maximum. Figure 11 shows the radial position error in the calibration points seen by the on-board camera in *p6* calculated with the rotation centre ~~of rotation~~ determined with the least square method.

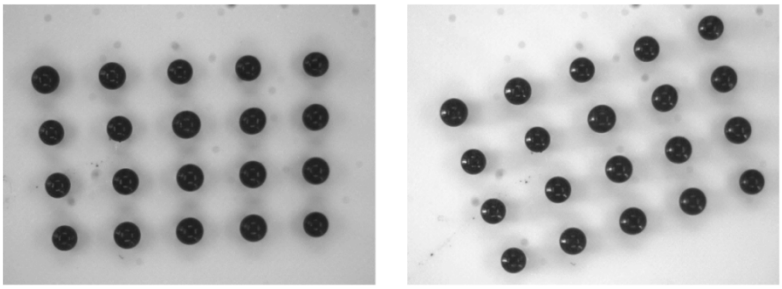

(a) (b)

Fig. 10. ~~The~~ I~~i~~mages of the grid taken from two different gripper positions: a) pose 1; b) pose 6.

Table IV. RMS error in the cross-reference test for the calculation of the rotation centre ~~of rotation~~.

E_{rms} [µm]	*c**	*c2*	*c3*	*c4*	*c5*	*c6*	*min*	*max*
p2	26.2	16.6	24.3	30.4	21.0	25.3	16.6	30.4
p3	22.5	41.1	20.4	27.6	23.2	28.3	20.4	41.1
p4	28.1	79.2	36.1	23.4	49.0	35.6	23.4	79.2
p5	18.8	20.7	17.1	21.7	16.2	20.3	16.2	21.7
p6	20.1	33.6	22.9	22.2	25.5	17.7	17.7	33.6

Table V. Maximum error in the cross-reference test for the calculation of the rotation centre ~~of rotation~~.

E_{max} [µm]	*c**	*c2*	*c3*	*c4*	*c5*	*c6*	*min*	*max*
p2	46.1	35.0	42.2	51.2	36.8	46.5	35.0	51.2
p3	45.4	77.3	42.9	51.6	53.8	55.3	42.9	77.3
p4	61.7	121.9	72.2	46.3	88.3	69.0	46.3	121.9
p5	45.6	42.0	41.0	50.2	42.2	47.9	41.0	50.2
p6	51.9	65.5	58.4	49.8	62.3	44.1	44.1	65.5

Table VI. Mean error in the cross-reference test for the calculation of the rotation centre ~~of rotation~~.

E_{mean} [µm]	*c**	*c2*	*c3*	*c4*	*c5*	*c6*	*min*	*max*
p2	23.9	14.3	22.1	28.2	18.9	23.1	14.3	28.2
p3	20.1	38.2	17.8	25.3	20.5	25.4	17.8	38.2
p4	24.9	77.1	33.1	20.7	46.3	31.3	20.7	77.1
p5	15.3	18.5	13.0	18.8	12.1	17.6	12.1	18.8
p6	16.9	31.6	20.1	19.2	22.9	14.3	14.3	31.6

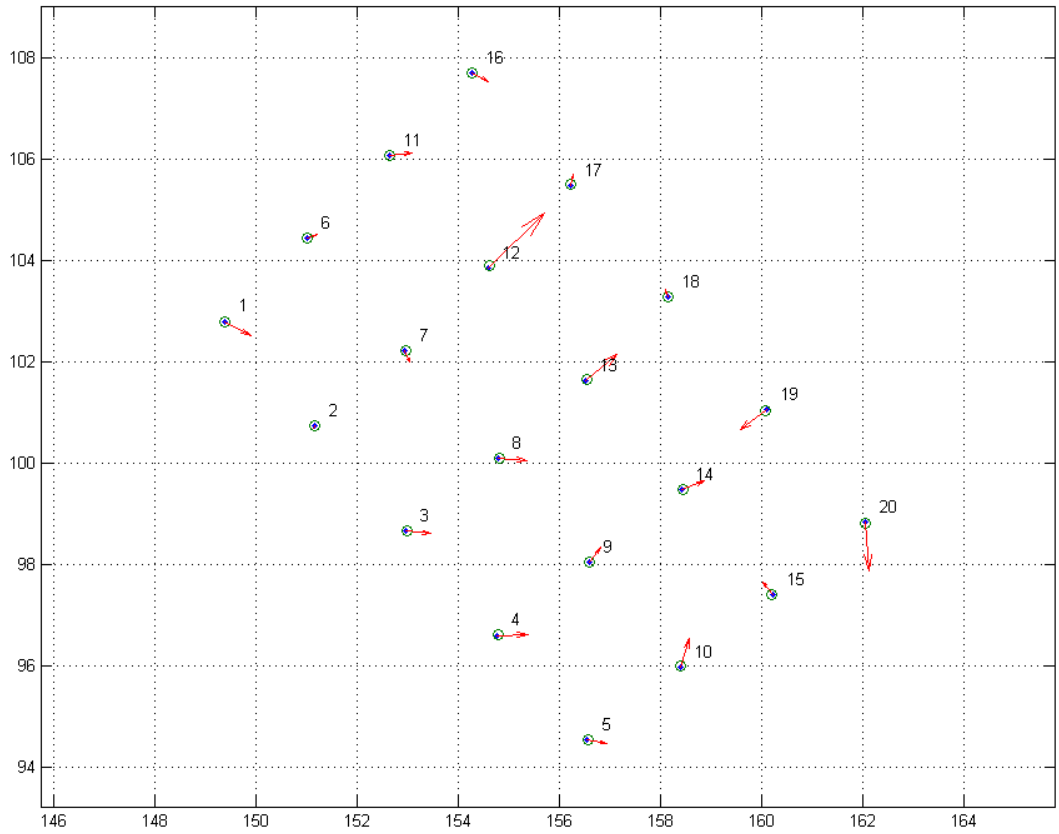

Fig. 11. Representation of ~~the~~ radial position error in the calibration points seen by ~~the~~ an on-board camera in *p6*.

In the virtual grid calibration strategy, ~~the~~ camera calibration and its registration are performed simultaneously, as in the previous cases. Different sources of error have to be considered. Since this procedure is similar to ~~that~~ the one of the second vision system looking at area2, all the errors arising in that case apply to this case. Moreover, since the camera moves with the robot, the robot pose accuracy influences the results. Indeed, ~~the~~ camera calibration is performed in a limited robot working area~~,~~ but ~~it~~ is then exploited in the whole area, where the robot performance can change. For this reason, differently from the case of fixed cameras, the virtual grid method applied to the on-board camera cannot compensate for even small errors correlated with ~~the~~ robot accuracy. Therefore, to guarantee the method precision ~~of the method a~~ preliminary robot calibration is needed.

8. E~~The e~~nd-effector calibration

When the robot is commanded to pick or release a part with a different orientation with respect to ~~that~~ the one adopted to calibrate the camera, a position error can be observed.

It was verified that the error ~~was~~ is due to a geometric error of the gripper (Fig. 12). Therefore, an easy and effective kinematic calibration of the robot end-effector ~~was~~ is devised to enhance accuracy (main idea iii in Section 1). This calibration exploit~~sed~~ the setup available in area1 able to provide a microgripper bottom view ~~of the microgripper~~. Indeed, the already calibrated and georeferenced camera 1 ~~was~~ is considered as a suitable measurement system for the robot end-effector position.

It is worth ~~to note~~noting that ~~the~~ gripper calibration ~~of the gripper~~ can be performed after the calibration of the vision systems, because in these cases ~~the~~ manipulation operations are performed with a fixed orientation of the gripper. The gripper errors ~~of the gripper~~ are simply compensated by an extra *x*-*y* translation with an amplitude depending on the gripper orientation.

In the following, the error model is reported together with ~~and the~~ experimental implementation and results ~~are reported~~.

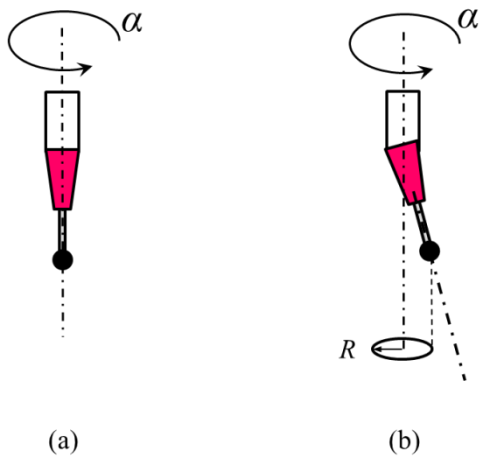

Fig. 12. The end-effector error: (a) ideal model; (b) error affected model.

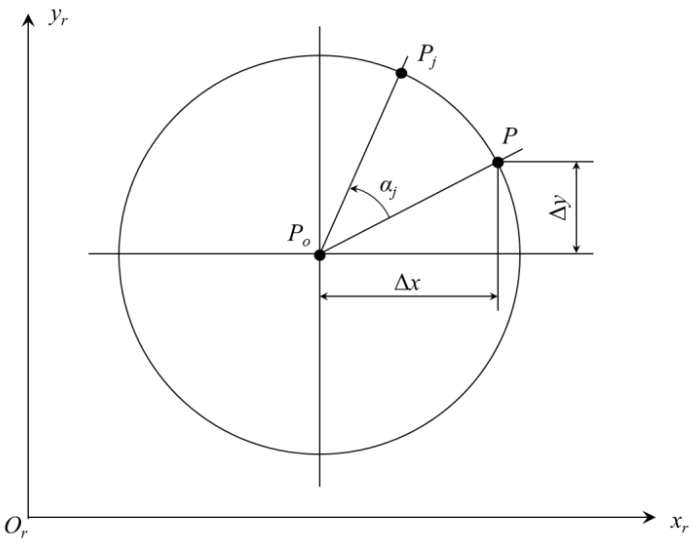

Fig. 13. Reference model for ~~the~~ end-effector calibration.

8.1 The error model

Misalignment and orientation errors with respect to the manipulator vertical rotational axis ~~of the manipulator~~ can affect the microgripper, thus causing inaccurate manipulation of ~~the~~ microcomponents. Figure 12 compares the ideal and the actual cases. In the former case, when commanding an α rotation ~~α~~ about the vertical axis of the robot, a simple rotation of the microgripper is obtained; ~~;~~ therefore there is no~~t~~ displacement in the *x*-*y* plane. In latter case, since the gripper centre does not belong to the rotation axis, ~~the~~ gripper rotation induces a displacement in the *x*-*y* plane.

Following an analysis of ~~Analysing~~ the system, the use of a rigid model to describe ~~the~~ gripper deformation ~~was~~ is considered as suitable. If a set of angular displacements ~~are~~ is commanded by keeping ~~constant~~ the end-effector *x*, *y* and *z* ~~the~~ position**s** constant ~~*x*, *y* and *z* of the end effector~~, the gripper nozzle barycentres (or the picked sphere barycentres) detected by the vision system 1 should lay on a circumference whose centre belongs to the vertical axis. Therefore, it is possible to derive a reference model as ~~that~~ the one shown in Fig. 13, where the bottom view of the robot end-effector by vision system 1 is considered.

Indicating with α_{cal} the end-effector rotation angle used during the camera calibration process and with $P = [x, y]^T$ the corresponding planar position of the end-effector, lying on the circumference of radius R and centre $P_o = [x_o, y_o]^T$ belonging to the rotation vertical axis:

$$\begin{bmatrix} x \\ y \end{bmatrix} = \begin{bmatrix} x_o \\ y_o \end{bmatrix} + \begin{bmatrix} \Delta x \\ \Delta y \end{bmatrix}$$

where Δx and Δy represent the microgripper misalignment ~~of the microgripper~~ with respect to P_o when $\alpha = \alpha_{cal}$.

~~Now consider~~If we ~~to~~ rotate the end-effector of the angle α_j relative to α_{cal}~~,~~ ~~it~~ this will achieve the new position $P_j = [x_j, y_j]^T$:

$$\begin{bmatrix} x_j \\ y_j \end{bmatrix} = \begin{bmatrix} x_o \\ y_o \end{bmatrix} + \begin{bmatrix} \cos(\alpha_j) & -\sin(\alpha_j) \\ \sin(\alpha_j) & \cos(\alpha_j) \end{bmatrix} \begin{bmatrix} \Delta x \\ \Delta y \end{bmatrix}$$

Thus, the position error ΔP_j due to the misalignment results as:

$$P_j - P = \begin{bmatrix} \Delta x_j \\ \Delta y_j \end{bmatrix} = \begin{bmatrix} \cos(\alpha_j) - 1 & -\sin(\alpha_j) \\ \sin(\alpha_j) & \cos(\alpha_j) - 1 \end{bmatrix} \begin{bmatrix} \Delta x \\ \Delta y \end{bmatrix}$$

Or, shortly, as:

$$\Delta P_j = A_i \begin{bmatrix} \Delta x \\ \Delta y \end{bmatrix}$$

In such model~~,~~ Δx and Δy are unknown constant parameters to be estimated for compensating for the described error with no hardware changes and enhancing the system accuracy. The parameters actual values ~~of the parameters~~ can be determined by applying the Least Square Method to a set of different achieved positions on the circumference. It is possible to group the measure of the gripper position error for n points as:

$$\Delta P = \begin{bmatrix} \Delta P_1 \\ \vdots \\ \Delta P_i \\ \vdots \\ \Delta P_n \end{bmatrix} \qquad A = \begin{bmatrix} A_1 \\ \vdots \\ A_i \\ \vdots \\ A_n \end{bmatrix}$$

and to solve the system with the least square criteria as:

$$\begin{bmatrix} \Delta x \\ \Delta y \end{bmatrix} = A^{+} \Delta P$$

It is worth ~~to note~~noting that by increasing the number of the rotations and ~~of~~ the considered points, a better estimation could be obtained.

8.2 Experimental implementation and results

The robot end-effector ~~was~~ is rotated over 360° with a step of 20°~~;~~, this means that ~~is~~ 18 rotations about the vertical axis ~~were~~ are performed. The previously executed camera calibration ~~previously executed could~~ cannot~~not~~ completely eliminate the errors in the image acquired by the camera ~~completely~~, therefore it ~~was~~ is decided that ~~to repeat~~ the series of rotations are repeated in a number of different positions in the camera FoV, trying to improve the ~~performance of the~~ calibration process performance. For this reason, a grid of 30 positions (6x5) ~~was~~ is chosen. The process steps ~~in the process were~~are:

1. the end-effector holding a sphere ~~was~~ is commanded to the first grid position with the angle used for ~~the~~ camera 1 calibration;
2. ~~the~~ C~~c~~amera 1 ~~took~~ takes a picture of the sphere, calculate~~d~~ and record~~ed~~ its position;
3. the end-effector rotated of the specified step angle (20°);
4. steps (2) and (3) ~~were~~ are repeated to span 360°;
5. the end-effector ~~was~~ is moved to the second (or the following) grid position with the calibration angle;
6. steps (2) to (5) ~~were~~ are repeated until the last rotation in the last grid position.

An over-constrained system of equations is obtained by rewriting the equation of ΔP_j for all the considered gripper poses. The system is linear in the unknowns Δx and Δy~~;~~ ~~thus~~ as a result they can be easily estimated by the Least Mean Square method (see Table VII). This makes the compensation of their effect possible by means of a geometric model.

In order to assess the calibration process effectiveness, the final mean, maximum and RMS position error values ~~were~~ are measured before and after the correction in 30 positions different from ~~those~~ the ones chosen for the calibration process and scattered in the working area (Fig. 14). Table VIII shows the ~~obtained~~ results obtained: in particular, the first three columns in the table report the errors that would be obtained if a position ~~were~~ is achieved with different orientations ignoring the correction. As one can see, the errors without the use of the end-effector calibration are an order of magnitude higher than ~~those~~ the ones with the end-effector calibration. Thus, a significant enhancement of the performance ~~was~~ is achieved.

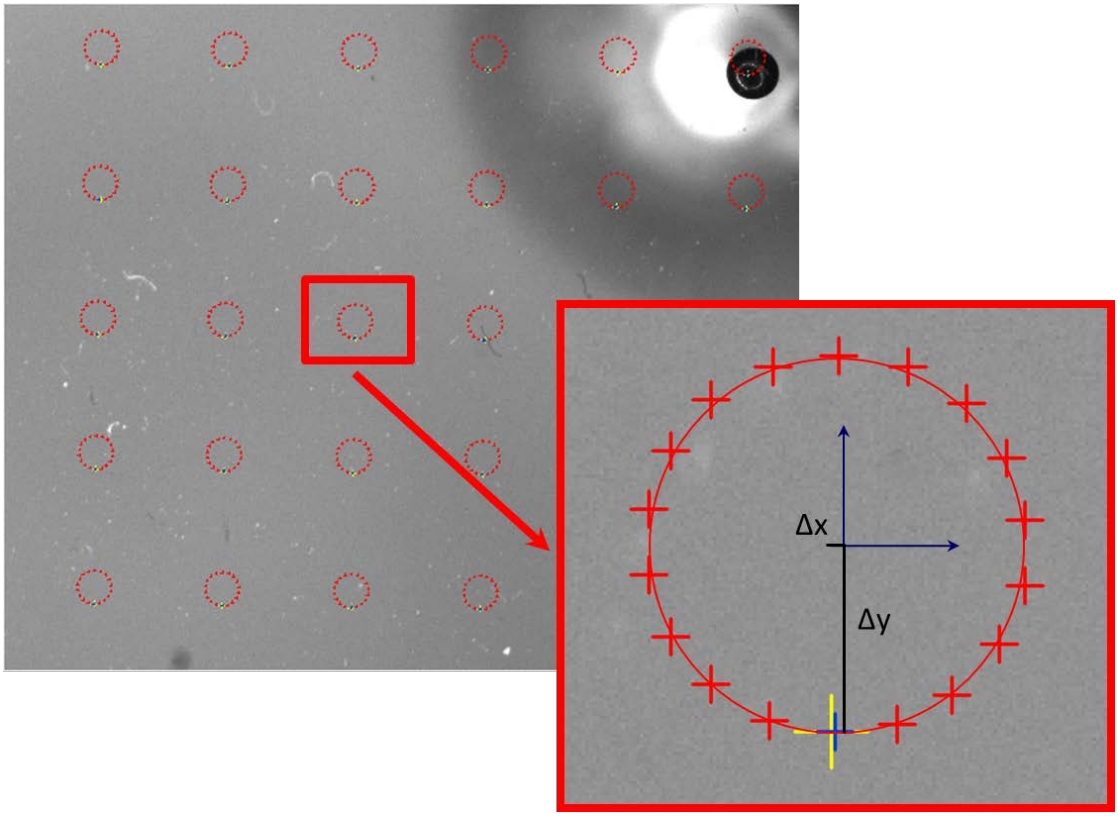

Fig. 14. The experimental points considered in the end-effector calibration ~~of the end-effector~~.

Table VII. Estimated values of ~~the~~ end-effector calibration parameters.

Δx [µm]	Δy [µm]	$R = \sqrt{\Delta x^2 + \Delta y^2}$ [µm]
-68.7	137.2	153.44

Table VIII. Results of ~~the~~ end-effector calibration (in all, two grids of 30 positions each and 18 rotations per position ~~were~~ are considered).

Error before calibration [µm]			Error after calibration [µm]		
Mean error	Max error	RMS error	Mean error	Max error	RMS error
188.8	309.3	109.7	11.8	30.0	6.2

An important aspect is represented by the need of a calibrated vision system to support the actual implementation of ~~the~~ end-effector calibration. Thus, both from ~~the~~ a conceptual and an operational point~~s~~ of view, ~~the~~ end-effector calibration ~~was~~ is addressed subsequent to the calibration of ~~the~~ area1. For this reason, the main error source is ~~the~~ area1 calibration error, which adds to the errors due to the encoder resolution, robot geometric errors, ~~the~~ vision algorithm performance and ~~the~~ auto-centring of the sphere

(when ~~the~~ a sphere is used).

The execution time of ~~the~~ end-effector calibration can take several minutes: for example, a 6x5 grid with 18 rotations for each position can be executed in 12-13 minutes. Obviously, as the number of points in the calibration grid or the step in the series of the end-effector rotations increase~~s~~, ~~the~~ time will increase proportionally. However, the number of points can be reduced.

9. Conclusions

This paper present~~sed~~ different calibration strategies applied to a micromanipulation work-cell. Two methods for ~~the~~ camera calibration and ~~the~~ camera-robot registration ~~were~~ are compared and critically analysed. The virtual grid approach demonstrate~~sd~~ higher efficiency ~~than~~ as compared to the hybrid calibration strategy, both from ~~the~~ a performance and an economic point~~s~~ of view. Indeed, the mean error in verification positions with the virtual grid approach ~~was~~ is less than half ~~that~~ compared to the one obtained with the hybrid approach, and the equipment price ~~of the equipment~~ (i.e. some glass spheres) ~~was~~ is two orders of magnitude ~~less~~ lower than ~~that~~ the one of a commercial grid. Moreover, the developed kinematic end-effector calibration procedure allow~~sed~~ for a significant improvement of the overall system accuracy: the error decrease~~sd~~ more than an order of magnitude. The ~~proposed~~ techniques proposed are general and can be applied to general micromanipulation work-cells that use robots up to 4 degrees of freedom and fixed or mobile 2D vision systems. In particular, the implementation of these calibration techniques has been preparatory for the execution of different micromanipulation and microassembly tasks, such as the mounting of mechanical microcomponents, the placement of electronic components on printing circuit boards, and the testing of microgrippers to evaluate their performance.

~~The~~ C~~c~~alibration procedures ~~did~~ do not require any additional equipment, as they exploit~~ing~~ only ~~the~~ micromanipulation work-cell devices: a robot, a gripper~~,~~ and vision systems, together with auto-centring objects (e.g. microspheres) to be manipulated. On the contrary, the laser sensor used to assure the orthogonality of the planes~~,~~ and the optical calibration grid necessary to perform the hybrid calibration~~,~~ are optional devices. This benefits the work-cell ~~the~~ overall cost ~~of the work-cell~~ since they are task-specific and can be rather expensive.

Acknowledgements

Thise work has been partially funded by the Italian Ministry for University and Research (MIUR) and by the Regione Lombardia under the framework of the 3AQ Regione Lombardia-CNR.

References

1. J. Cecil, M.B. Bharathi Raj Kumar, Y. Lu, and Vinod Basallali, “A review of micro-devices assembly techniques and technology”, *The International Journal of Advanced Manufacturing Technology*, Vol. 83, Issue 9, pp.1569-1581 (2016).
2. K. Schröer, “Precision and calibration”, in *Handbook of Industrial Robotics*, 2nd edition, Wiley & Sons Inc., New York. Edited by Shimon Y. Nof (1999).
3. G. Legnani, C. Mina and J. Trevelyan, “Static calibration of industrial manipulators: Design of an optical instrumentation and application to SCARA robots”, *Journal of Robotic Systems*, Vol. 13, No. 7, pp. 445-460 (1996).
4. A. Omodei, G. Legnani and R. Adamini, “Calibration of a measuring robot: Experimental results on a 5 DOF structure”, *Journal of Robotic Systems*, Vol. 18, No. 5, pp. 237-250 (2001).
5. B.W. Mooring, Z.S. Roth and M.R. Driels, “Fundamentals of manipulator calibration”, *John Wiley & Sons, Inc. New York* (1991).
6. Z. Zhang, “A flexible new technique for camera calibration”, *IEEE Transactions on Pattern Analysis and Machine Intelligence*, Vol. 22, No. 11, pp. 1330-1334 (2000).
7. J. G. Fryer and D. C. Brown, “Lens distortion for close-range photogrammetry”, *Photogrammetric Engineering and Remote Sensing*, Vol. 52, pp.51–58 (1986).
8. S. Ruggeri, G. Fontana, I. Fassi. “Chapter 9: Micro-assembly”, in *Micro-Manufacturing Technologies and Their Applications: A Theoretical and Practical Guide*, Springer. Edited by. I. Fassi and D. Shipley (2017). In press
9. G. Fontana, “Assembly at the microscale: design and implementation of a robotised work-cell”, *PhD Thesis*, University of Brescia (2014).
10. S. Ruggeri. “Advanced robotic applications: performance improvement techniques for industrial robots acting at the macro- and micro-scale”, *Scholar’s Press*, Germany (2013).
11. Mitsubishi website: *http://www.mitsubishi-automation.co.uk/*.
12. O. Bottema and B. Roth, “Theoretical kinematics”, *Dover Publications Inc.*, New York, pp. 312–315 (1979).
13. G. Legnani, A. Gabrielli, A. Ousdad, I. Fassi, S. Ruggeri and G. Fontana, “A Laser Calibration Device for Mini Robots”, in *Proceedings of the ASME 2015 International Design Engineering Technical Conferences & Computers and Information in Engineering Conference IDETC/CIE 2015*, Boston, Massachusetts, USA (2015).
14. ISO 9283:1998 “Manipulating industrial robots - Performance criteria and related test methods” (1998).
15. ISO/TR 13309:1995 “Manipulating industrial robots - Informative guide on test equipment and

metrology methods of operation for robot performance evaluation in accordance with ISO 9283" (1995).
16. B. Tamadazte, S. Dembélé, N. Le Fort-Piat, "A Multiscale Calibration of a Photon Videomicroscope for Visual Servo Control: Application to MEMS Micromanipulation and Microassembly", *Sensors & Transducers Journal*, Vol. 5, Special Issue, pp. 37-52 (2009).
17. G. Bradski and A. Kaehler, "Learning OpenCV", *O'Reilly* (2014).
18. I. Fassi, and G. Legnani, "Hand to sensor calibration: A geometrical interpretation of the matrix equation AX=XB", *Journal of Robotic Systems*, Volume 22, Issue 9, pages 497–506 (2005).
19. I. Fassi, G. Legnani, D. Tosi and A. Omodei, "Chapter 8: Calibration of Serial Manipulators: Theory and Applications", in *Industrial Robotics: Programming, Simulation and Applications*, Intech. Book. Edited by Low Kin Huat (2006).
20. G. Legnani, D. Tosi, R. Adamini and I. Fassi, "Chapter 9: Calibration of Parallel Kinematic Machines: Theory and Applications", in *Industrial Robotics: Programming, Simulation and Applications*, Intech. Book. Edited by Low Kin Huat (2006).
21. L. G. Shapiro and G. C. Stockman, "Computer Vision", *Englewood Cliffs*, NJ: Prentice-Hall (2002).

Appendix A: Manipulator Errors

Errors in the manipulator structure determine an error in the gripper pose that can be represented mainly by two performance indexes: accuracy and repeatability [14]. Accuracy depends on constant sources of errors like geometric inaccuracy and encoders offset, ~~while~~ whereas repeatability is affected by random errors (mainly mechanical backlash). Accuracy errors can be predicted and compensated by suitable calibration techniques [3, 4, 5], in order to get closer to the application desired final precision ~~of the application~~. In general, the end-effector ~~the~~ pose (position and orientation) S ~~of the end effector~~ can be expressed in function of the joint coordinate vector Q and of the structural parameters L as:

$$S = f(Q, L) \cong f(Q_n, L_n) + \frac{\partial f}{\partial Q}\Delta Q + \frac{\partial f}{\partial L}\Delta L$$

where f is the direct kinematics function, the subscript n marks the nominal values and Δ marks the deviation from the nominal situation. On the basis of suitable models [19, 20] and of experimental data, it is possible to estimate the error ΔL of the unknown parameters and compensate for them with a suitable variation of the joint coordinates ΔQ. ~~The~~ Cealibration can be performed by the final user~~,~~ or directly at the factory by the manufacturer for an extra cost.

Appendix B: Camera and Lens Distortion Models

Perspective errors occur when the camera axis is not orthogonal to the object under inspection. To limit the perspective error, the camera should be positioned ~~the most~~as orthogonally as possible to the planar surface, however this error has to be compensated to compute the image pixel to real-world unit transformation. Moreover, distortion errors are introduced by lens imperfections. Typically, a camera lens introduces radial distortion, that is the image information is misplaced relatively to the optical centre of the lens [7].

Since cameras can be described by the pin-hole model [21], the 2D perspective correction is based on the following equations:

$$\begin{cases} x = \dfrac{au'+bv'+c}{gu'+hv'+1} \\ y = \dfrac{du'+ev'+f}{gu'+hv'+1} \end{cases} \qquad (B1)$$

where, after the distortion correction, x and y represent the position in the real world of one feature in the image whose coordinates in pixels are u' and v', and a, b, c, d, e, f, g, h are suitable constants to be determined by calibration.

The optical distortion [17] can be modelled by suitable polynomials in the distance r of the considered image point from the centre of distortion u_c, v_c:

$$\begin{bmatrix} u' \\ v' \end{bmatrix} = \begin{bmatrix} u \\ v \end{bmatrix} + \left(1 + k_2 r^2 + k_4 r^4 + \cdots\right) \begin{bmatrix} u'' \\ v'' \end{bmatrix} + \begin{bmatrix} 2a'v''+b'\left(r^2+2u''^2\right) \\ 2a'\left(r^2+2v''^2\right)+2b'u'' \end{bmatrix} \qquad r^2 = u''^2+v''^2 \qquad \begin{bmatrix} u'' \\ v'' \end{bmatrix} = \begin{bmatrix} u-u_c \\ v-v_c \end{bmatrix} \qquad (B2)$$

where k_{2i} ($i \in \mathrm{N}^*$) and a' and b' are constants to be experimentally determined.